# Let it bud: an ultrastructural study of *Cryptococcus neoformans* surface during budding events

Glauber R. de S. Araújo[1], Carolina de L. Alcantara[1], Noêmia Rodrigues[1] Wanderley de Souza[1,3], Bruno Pontes[2,3†] & Susana Frases[1†]

[1] Laboratório de Ultraestrutura Celular Hertha Meyer, Instituto de Biofísica Carlos Chagas Filho, Universidade Federal do Rio de Janeiro, Rio de Janeiro, RJ, Brazil.

[2] Laboratório de Pinças Óticas (LPO-COPEA), Instituto de Ciências Biomédicas, Universidade Federal do Rio de Janeiro, Rio de Janeiro, RJ, Brazil.

[3] Centro Nacional de Biologia Estrutural e Bioimagem (CENABIO), Universidade Federal do Rio de Janeiro, Rio de Janeiro, RJ, Brazil.

[†] These authors share the senior position

Susana Frases ✆ +55 (21) 3938-6593 ✉ susanafrases@biof.ufrj.br

Bruno Pontes ✆ +55 (21) 3938-6465 ✉ bpontes@icb.ufrj.br

Keywords: *Cryptococcus neoformans*; Polysaccharide capsule; Cell wall; Budding; Electron microscopy.

## Abstract

*Cryptococcus neoformans* is a fungal pathogen that causes life-threatening infections in immunocompromised individuals. It is surrounded by three concentric structures that separate the cell from the extracellular space: the plasma membrane, the cell wall and the polysaccharide capsule. Although several studies have revealed the chemical composition of these structures, little is known about their ultrastructural organization and remodeling during *C. neoformans* budding event. Here, by combining the state-of-the-art in light and electron microscopy techniques we describe the morphological remodeling that occurs synergistically among the capsule, cell wall and plasma membrane during budding in *C. neoformans*. Our results show that the cell wall deforms to generate a specialized budding region at one of the cell's poles. This region subsequently begins to break into layers that are slightly separated from each other and with thick tips. We also observe a reduction in density of the capsular polysaccharide around these specialized regions. Daughter cells present a distinct spatial organization, with polysaccharide fibers aligned in the direction of budding. In addition, to control the continuous openings between mother and daughter cells, the latter developed a strategy to shield themselves by forming multilamellar membrane structures in conjunction with their capsules. Together, our findings provide compelling ultrastructural evidence for a dynamic *C. neoformans* surface remodeling during budding and may have important implications for future studies exploring these remodeled specialized regions as drug-targets against cryptococcosis.

## 1. Introduction

Fungal infections that cause systemic mycoses have become a major threat, a clinical and a pharmaceutical challenge since the end of the 20$^{th}$ century, especially affecting individuals with an immunological impairment (Perfect, 2013). There are evidences showing that the increase in fungal infections might be correlated with glucocorticoid therapy, immunotherapy, oncological and hematological diseases, increased number of transplants, surgical procedures, individuals living with acquired immunodeficiency syndrome (AIDS), among others (Henao-Martínez and Beckham, 2015; Liao et al., 2016; Singh et al., 2008).

*Cryptococcus* spp., of which *Cryptococcus neoformans* is the main representative of the genus, is a basidiomycete that presents itself as a haploid and spherical yeast surrounded by a polysaccharide (PS) capsule, a unique feature among eukaryotes (D. McFadden et al., 2006). These cells commonly have an average diameter ranging from 2 to 8 μm; however, under certain conditions of physical and/or chemical stresses, they can reach up to 100 μm in diameter, the so-called "titan cells" (Faganello et al., 2006; Trevijano-Contador et al., 2018; Zaragoza, 2019; Zaragoza et al., 2003). *Cryptococcus* spp. has a global distribution and causes about 625,000 deaths per year worldwide (Park et al., 2009). The host becomes infected after inhaling spores or desiccated yeasts (Ellis and Pfeiffer, 1990) and the infection can either take its latent form, without causing any clinical symptoms, or manifest itself in the acute form of the disease (Goldman et al., 2010). Given that *Cryptococcus* spp. has a special tropism toward the Central Nervous System (CNS) and can colonize the CNS through many concomitant infection routes (Mitchell et al., 1995), one can consider cryptococcal meningitis as the most severe cryptococcosis scenario (Casadevall and Perfect, 2008).

The success of the infection is based on the ability of the fungus to evade the host's immune system. During its evolution, *Cryptococcus* spp. developed several adaptation mechanisms, known as virulence factors. Some examples are: **(I)** melanin production and cell wall remodeling (resistance to cell-mediated death and immunomodulation) (Doering et al., 1999; Gómez and Nosanchuk, 2003; Huffnagle et al., 1995; Liu et al., 1999; Wang et al., 1995), **(II)** production of superoxide dismutase (protection against toxic free radicals) (Cox et al., 2003) **(III)** phospholipase and urease secretion (intracellular growth, diffusion and proliferation) (Cox et al., 2001, 2000) **(IV)** phenotypic switching (immune evasion) (Fries et al., 2001; Goldman et al., 1998), **(V)** cellular gigantism (immune evasion) (Okagaki et al., 2010; Trevijano-Contador et al.,

2018; Zaragoza, 2019; Zaragoza and Nielsen, 2013) and **(VI)** PS production, which is the main virulence factor used by *C. neoformans* (Araujo et al., 2012; Zaragoza, 2019; Zaragoza et al., 2009). Most of these features are believed to have been acquired through selective pressures and are likely to be the result of interactions with environmental predators, such as amoebae and nematodes (Albuquerque et al., 2019; Casadevall and Pirofski, 2007).

After production, *Cryptococcus* spp. PS can be either secreted to the extracellular milieu through vesicles (Rodrigues et al., 2007) or transported to the cell wall where it forms the physical structure of the capsule *in situ*. Depending on its fate, PS acquires different physicochemical and rheological properties (Araújo et al., 2019; Pontes and Frases, 2015; Zaragoza, 2019). Due to its unique morphology and the fact that it is pivotal for the establishment of pathogenesis, the PS capsule is the most distinctive feature of the *Cryptococcus* genus. It is highly dynamic, extremely hydrophilic and can be modified in response to the environment. This structure appears at the surface of the cell wall and its main roles are to protect the cell against host's defense factors and to interfere with immune response mechanisms (Perfect and Casadevall, 2011). In order to anchor to the cell wall, the PS molecules from the capsule interact with α-1,3 glucans (Reese and Doering, 2003). However, the full mechanism that dictates the interaction between capsule and cell wall is far from being completely understood but is thought to involve molecular interactions between the components of both structures.

The fungal cell wall is an intricate network of macromolecules such as lipids, proteins and other polymers like glucans, mannans, galactomannans and chitin. This structure is considered to be a primary determinant of the fungi resistance to stress and environmental aggressions. It provides not only strength and rigidity to maintain the cell conformation but also flexibility to support morphological changes, such as cell growth and budding (Adams, 2004; Roncero, 2002; Ruiz-Herrera et al., 2002). The cryptococcal cell wall also serves as the scaffold for the assembly/anchoring of the PS capsule. Genetic interruptions of its synthesis reduce cell viability and decrease capsule assembly, often producing avirulent mutants. These features make the capsule an attractive target for the development of antifungal therapies, especially because mammalian cells do not have equivalent structures (Wang et al., 2018).

The cell wall is comprised by a matrix containing glycoproteins and glucose (Glc), *N*-acetylglycosamine (GlcNAc) and glucosamine (GlcN) polymers, whose main constituents are glucans, chitin and chitosans (Perfect and Casadevall, 2011). The glucans

are divided into α- and β-glucans. A large fraction of α- glucans present α-1,3 links (Bose et al., 2003; James et al., 1990; Wang et al., 2018) whereas the majority of β-glucans are comprised by β-1,3 and β-1,6 bonds (James et al., 1990; Manners et al., 1973; Wang et al., 2018). Chitin, another constituent of the cell wall, is a water-insoluble β-1,4-GlcNAc polymer, that associates with one another to form chitooligomers (chitooligosaccharides). These chitooligomers contain between three to twenty residues of β-1,4-GlcNac, which provides the cell wall with rigidity and structural integrity under various environmental conditions. In *C. neoformans*, chitooligomers are also incorporated into the capsular network and interact with glucuronoxylomannan (GXM) to form complex glycans. Chitin-derived oligomers have also been shown to regulate capsular architecture in *C. neoformans* cells, playing an indirect role in cryptococcal pathogenesis. Finally, they were also detected at the capsular surface, suggesting their potential to be recognized by host receptors, possibly affecting cryptococcal pathogenesis (Fonseca et al., 2013). Cell wall chitins can also be deacetylated to generate chitosan, a more soluble and flexible glucosamine polymer. *C. neoformans* have high levels of chitosan that can exceed chitin amounts up to 10 times (Banks et al., 2005). Cells without chitosan grow slower than the wild type and present impaired cell integrity and reduced virulence in animal models (Baker et al., 2011). Overall, glycoproteins are crucial components of the cell wall in fungi, as they act in critical processes, including signal transduction, conjugation, cell wall synthesis and iron acquisition. These proteins are modified by *N*-oligosaccharide and *O*-oligosaccharide bonds, usually mannosylated structures, which syntheses are initiated in the endoplasmic reticulum and in the Golgi complex (Wang et al., 2018). Glycans linked to the cryptococcal proteins contain xylose (Xyl) and Xyl-phosphate moieties (Lee et al., 2015; Park et al., 2012; Reilly et al., 2011). Even though the full spectrum of glycans has not yet been completely elucidated, it is known that it contains sialic acid that plays an anti-phagocytic role and may represent a virulence factor in the initial stages of infection (Rodrigues et al., 2002).

Since the last century there has been a great interest in deciphering the chemical composition of *C. neoformans* cell surface; however, little is known about its ultrastructural organization and remodeling during important events of *C. neoformans* biology. In the present work, we combined the most up-to-date light and electron microscopy techniques to describe the morphological remodeling that synergistically occurs between the capsule, the cell wall and the plasma membrane during the budding phenomenon in *C. neoformans*.

## 2. Materials and Methods

### 2.1 Microorganisms

The strain used in this work was *C. neoformans* var. *grubii* H99 (clinical isolate, kindly provided by Professor Arturo Casadevall - Johns Hopkins Bloomberg School of Public Health, Baltimore, Maryland, USA), a wild type strain available in the American Type Culture Collection (ATCC catalog number 208821).

### 2.2 Capsule induction and culture conditions

Yeasts were grown in Sabouraud Dextrose Broth (Kasvi, PR, Brazil) medium at 37$^{o}$C with constant agitation at various times, depending on the experimental conditions. For video microscopy observations, the yeasts were taken directly from Sabouraud Dextrose Agar (Kasvi, PR, Brazil) and, subsequently, added in liquid culture medium and processed, as described below. In order to induce capsule formation, the yeasts were kept at 37$^{o}$C for 7 days in a nutrient-deprived medium called Minimal Medium (MM) containing only 15 mM glucose, 10 mM $MgSO_4 7.H_2O$, 29 mM $KH_2PO_4$, 13 mM glycine and 3 µM thiamine (all compounds from Merck Millipore, Darmstadt, Germany).

### 2.3 Video microscopy

An initial inoculum of $10^4$ cells/mL in Sabouraud medium was added to 35 mm glass bottom dishes (Thermo Scientific ™ Nunc Glass Bottom Dish, Waltham, MA, USA) and observed under a Nikon Eclipse TE300 inverted microscope equipped with a CFI Achromatic LWD ADL 40X objective lens. For 5 hours, phase contrast images were captured every minute using a Hamamatsu C2400 CCD camera (Hamamatsu, Japan). Images were then mounted into stacks and analyzed using the ImageJ 1.8.0 software (NIH, Bethesda, MD, USA - https://imagej.nih.gov/ij/) (Abràmoff et al., 2004; Schneider et al., 2012).

### 2.4 Conventional fluorescence microscopy and structured illumination microscopy (SIM)

Yeast cells ($10^6$) were centrifuged at 6,708 *g* for 5 minutes, resuspended in 4% (v/v) paraformaldehyde (Electron Microscopy Sciences, Hatfield, PA, USA) in phosphate buffered saline (PBS) (137 mM NaCl, 2.7 mM KCl, 10 mM $Na_2HPO_4$ and 1.8 mM

$KH_2PO_4$) pH 7.2 and incubated for 30 minutes at room temperature. Next, fixed cells were washed twice with PBS and incubated with 1% bovine serum albumin (Sigma Aldrich, Darmstadt, Germany) in PBS for 1 hour at room temperature. The cells were then incubated for another hour at room temperature with 18B7 mAb (10 µg/mL). The 18B7 mAb is a mouse IgG1 with high affinity for GXM from different cryptococcal serotypes (Goldman et al., 1998). After three washes in PBS, cells were incubated with 10 µL/mL of the anti-mouse Alexa Fluor® 594 secondary antibody (Thermo Fisher Scientific, Waltham, Massachusetts, USA) for 1 hour at room temperature. Again, cells were washed with PBS buffer and incubated with Uvitex2B (Polyscience Inc, Warrington, PA, USA) for 1 hour at room temperature and subsequently, vigorously washed 4 times with PBS buffer in order to remove all Uvitex2B dye to minimize background.

Cell suspensions were mounted on glass coverslips and observed using an Axio Observe or an Elyra PS.1 microscope (Zeiss, Germany). Images were acquired with their respective software packages and subsequently processed using ImageJ 1.8.0 software (NIH, Bethesda, MD, USA - https://imagej.nih.gov/ij/) (Abràmoff et al., 2004; Schneider et al., 2012) .

**2.5 Conventional scanning electron microscopy (CSEM)**

The cells of interest were washed three times in PBS pH 7.2 and fixed in 2.5% glutaraldehyde solution grade I (Electron Microscopy Sciences, Hatfield, PA, USA) in sodium cacodylate buffer 0.1 M pH 7.2 for 1 hour at room temperature. Then, the cells were washed three times in 0.1 M sodium cacodylate buffer pH 7.2 containing 0.2 M sucrose and 2 mM $MgCl_2$ (Merck Millipore Darmstadt, Germany), and adhered to 12 mm diameter round glass coverslips (Paul Marienfeld GmbH & Co. KG, Germany) previously coated with 0.01% poly-L-lysine (Sigma-Aldrich, Darmstadt, Germany) for 20 minutes. Adhered cells were then gradually dehydrated in an ethanol (Merck Millipore, Darmstadt, Germany) series (30, 50 and 70% for 5 minutes and 95% and 100% twice for 10 minutes). The dehydration procedure was meticulously monitored to prevent PS collapse during air drying or PS extraction due to excessive incubation. The coverslips were then critical-point-dried using an EM DPC 300 critical point drier (Leica, Germany) and mounted on specimen stubs using a conductive carbon adhesive (Pelco Tabs™, Stansted, Essex, UK). Next, the samples were coated with a thin layer of gold or gold-palladium (10-15 nm) using the sputter method (Balzers Union FL -9496, Balzers, FL). Finally, samples were

visualized in a scanning electron microscope (Zeiss Evo 10 or FEI Quanta 250) operating at 10-20 kV with an average working distance of 10 mm and images were collected with their respective software packages.

**2.6 High resolution scanning electron microscopy (HRSEM)**

The cells were processed following the same methodology described above (please, see CSEM). However, in order to proceed with HRSEM, the samples were sputtered with a 3 nm thick platinum layer on their surfaces and observed in high resolution electron microscopes, either FEI Magellan™ (FEI Company, Oregon, USA) or Zeiss Auriga-40 (Zeiss, Germany) operating at 1 kV with an average working distance of 2 mm and images were collected using their respective software packages.

Quantification of PS fiber anisotropy was performed using FibrilTool (Boudaoud et al., 2014), an ImageJ plug-in that determines the average orientation of a fiber array. The anisotropy value ranges from a maximum of 1, when all fibers point to the same direction, to a minimum of 0, when fibers are randomly oriented.

**2.7 Transmission electron microscopy (TEM)**

The cells were washed three times in PBS pH 7.2 and subsequently fixed in 2.5% (v/v) glutaraldehyde solution grade I in 0.1 M sodium cacodylate buffer pH 7.2 and microwaved (350 W, 3 pulses of 30 seconds each with an interval of 60 seconds between pulses) (Benchimol et al., 1993; Giberson et al., 2003). Subsequently, the cells were washed three times in 0.1 M sodium cacodylate buffer pH 7.2. The cells were then post-fixed using an Osmium-Thiocarbohydrazide-Osmium (OTO) protocol. Briefly, cells were incubated in a post-fixative 1% (v/v) osmium tetroxide ($OsO_4$), 0.8% (v/v) potassium ferrocyanide and 5 mM calcium chloride, in 0.1 M cacodylate buffer (pH 7.2) for 10 min, washed twice in water, and then incubated in 1% (w/v) thiocarbohydrazide (TCH, Sigma, Darmstadt, Germany) in water, for 5 min (Murakami et al., 1983; Seligman et al., 1966; Willingham and Rutherford, 1984). After three washes in water, cells were again incubated in the post-fixative osmium solution for 2 min and finally washed three times in water. Next, cells were gradually dehydrated in an acetone (Merck Millipore, Darmstadt, Germany) series: 50%, 70%, 90% and two subsequent 100%. All the dehydration procedures were performed in the microwave (350 W, 10 seconds pulses for each step). The Spurr resin (Electron Microscopy Sciences, Hatfield, PA) was gradually used to substitute acetone in the following proportions acetone: Spurr (v:v): 3:1, 2:1, 1:1,

1:2, 1:3 and finally pure Spurr. Each mixture was also submitted to the same microwave cycles for 2 minutes except the last step (pure Spurr) that was performed without any radiation. The polymerization step was carried out for 48 hours in an oven at 70ºC. The samples were sliced in 75 nm sections under a Leica EM UC7 ultramicrotome (Leica, Wetzlar, Germany), collected onto formvar-coated copper slot grids and submitted to an incubation with 5% (w/v) uranyl acetate in water for 20 minutes and lead citrate for 5 minutes for contrasting. Finally, the samples were observed in a Tecnai™ Spirit microscope operated at 120 kV (FEI Company, Oregon, USA) and images were collected using the microscope software.

### 2.8 Electron tomography and three-dimensional reconstruction

The samples were processed following the same procedures described above (see TEM). However, for electron tomography, a few different steps were performed, as follows. Samples were sliced into 200 nm thick serial sections under a Leica EM UC7 ultramicrotome (Leica, Wetzlar, Germany), collected onto formvar-coated copper slot grids and stained with 5% (w/v) uranyl acetate for 3 minutes and Reynolds' Lead citrate for 5 minutes. The tomographic series were acquired with an inclination of ± 65° and 1° increments under a Tecnai Spirit™ (FEI Company, Oregon, USA) transmission electron microscope operating at 120 kV with a 2,048 X 2,048 pixels' matrix CCD camera. Serial tilt series were aligned using Etomo, an open-source software from IMOD package, a set of image processing, modeling and display programs used for tomographic reconstruction and for 3D reconstruction of EM serial sections (Kremer et al., 1996; Mastronarde, 1997). Generated tomograms were reconstructed using 3dmod.

### 2.9 Statistical analysis

Statistical analysis were performed using GraphPad Prism 8.4.0 (GraphPad Software, La Jolla, CA). Student's *t*-test was used for comparisons.

## 3. Results

### 3.1 *Cryptococcus neoformans* differentiates a region of its cell wall to generate daughter cells.

*C. neoformans* divides through budding of daughter cells from mother cells (Lin et al., 2014). To revisit and better characterize this phenomenon, yeast cell cultures were grown in Sabouraud Dextrose Broth medium and were allowed to attach onto coverslips. Next, we acquired phase contrast images of the same field of view every minute for 5 hours. Images were mounted in stacks allowing us to follow the proliferative behavior of the cells. Mother cells (G1) generated their daughters (G1.1) at an average rate of one cell every (1.3 ± 0.3) h (Figure 1 and Supplementary Video 1). Moreover, successive daughter cells always bud from the same regions of their respective mothers, not only from cells that were attached since the beginning (Figures 1A, 1B and 1C and Supplementary Video 1), but also from daughter cells that subsequently attached to the coverslips after budding and also started to generate daughter cells of their own (Figures 1C and 1D and Supplementary Video 1).

Although this observation is already a consensus in the *Cryptococcus* field (Zaragoza et al., 2006a, 2006b) it led us to hypothesize that the mother cell might develop a specialization at the cell wall, creating a region with certain characteristics that might facilitate budding.

### 3.2 *Cryptococcus neoformans* mother cell wall reorganizes prior to budding of daughter cells.

In order to unravel details of these specialized regions (SRs), *Cryptococcus neoformans* yeast cell cultures were stained with Uvitex2B to label the chitin polymers present in the cell wall and subsequently were observed in a conventional fluorescence microscope. Images showed that mother cells, before budding of daughter cells, formed regions of lower fluorescence intensities when compared to the rest of the cell perimeter (Figures 2A, 2B and 2C).

In an attempt to better clarify the organization of these SRs, we also imaged *C. neoformans* cells using SIM. Uvitex2B was used together with 18B7 + Alexa Fluor® 594, to stain both the cell wall and the PS capsule respectively (Figure 3). The results confirmed the decrease in fluorescence intensities around the SR when compared to the entire cell perimeter (Figures 3A, 3B and 3C). Furthermore, although with few details, it was possible to identify that the cell walls seemed to peel off in order to form the SRs from which daughter cells bud. (Figure 3C and Supplementary Video 2).

### 3.3 Ultrastructural details of *C. neoformans* specialized regions during budding.

In order to better visualize the SRs with greater resolving power, we used transmission electron microscopy (TEM) and three-dimensional reconstruction by electron microscopy.

*Cryptococcus neoformans* yeast cell cultures were imaged using TEM. By using this technique, we were able to specifically follow the various steps of the budding process (Figures 4, 5 and 6). Our observations demonstrated that the process started with the shape change of one of the poles of the cell which deformed, lost sphericity and formed a more pointed region in the cell wall that, at some point, began to break into layers (Figures 4A and 4B). As the daughter cell started to appear, the formed layers became more evident with thick tips slightly separated from each other (Figures 4C and 4D). When the daughter cell is released, a new budding event is likely to arise in the same region as the first detached daughter cell turns the area more prone for subsequent occurrences (Figures 4E and 4F).

Electron tomography and three-dimensional reconstruction were also performed in order to enable us to observe further details about the budding events (Figure 5 and Supplementary Video 3). Strikingly, with the tomography series, it became clearer that not only there is a separation of the mother cell wall into layers with thick tips (Figures 5A and 5B), as previously described (Figure 4), but also that the mother cell wall is thicker than the daughter cell wall (Figure 5D). Interestingly, daughter cells presented multilamellar membranous structures that seem to cover the continuous openings between daughter and mother cells, as a protective barrier (Figure 5D and 5E). It also became evident that the entire budding process induced capsule reorganization around the SRs (Figures 4 and 5). The most striking changes observed in the capsule morphology during budding were the reduction in PS density around SRs (Figure 4) and the formation of a protective PS barrier surrounding the SRs of both mother and daughter cells (Figures 5C, 5D and 4E). Three-dimensional reconstruction clearly demonstrated all of these characteristics (Figures 5F and 5G).

Thus, cell wall structural reorganization and capsule remodeling are evident processes that occur in both mother and daughter cells during budding.

### 3.4 Capsule polysaccharide fibers around specialized regions of daughter cells are oriented towards the budding events.

In order to clarify the details of capsule remodeling and also to better understand the PS reduced density around the SRs, *C. neoformans* were processed and visualized by conventional and high-resolution scanning electron microscopes (Figure 6).

As previously described (Figures 4 and 5), the images presented in Figure 6 confirmed not only the remodeling but also the reduction in PS density around the SRs. Moreover, the PS fibers from daughter cells have a distinct spatial organization surrounding these SRs, with fibers aligned in the direction of budding (Figures 6A – 6E). In order to better quantify these visual observations, we performed a quantitative analysis using the FibrilTool plug-in (Boudaoud et al., 2014). The results (Figure 6F) showed that, overall, the PS fibers around SRs present a higher anisotropy when compared to fibers outside the SRs. This special arrangement around SRs may be related to the mechanical force that occurs during budding.

## 4. Discussion

*Cryptococcus neoformans* present themselves as haploid and spherical yeasts, surrounded by a PS capsule, unique feature among eukaryotes (D. C. McFadden et al., 2006). PS capsule in *C. neoformans* is its main virulence factor (Doering, 2000; Rodrigues et al., 2009; Zaragoza, 2019; Zaragoza et al., 2009), and it plays several roles, such as protection against dehydration and phagocytosis by natural predators in the environment. In addition, in the context of human infection, the PS capsule provides protection against phagocytosis, inhibition of leukocyte migration, depletion of the complement system and inhibition of antibody production (Dong et al., 1995; Feldmesser et al., 2001; Kozel et al., 1977; Macher et al., 1978; Murphy and Cozad, 1972; Retini et al., 1998; Zaragoza et al., 2009, 2008). Thus, the PS capsule becomes a primary component of interaction between the fungi and their host cells, using its immunomodulatory dynamics and its antiphagocytic properties to hinder the host's immune response, therefore becoming one of the main targets for therapeutic strategies (Casadevall and Pirofski, 2007; Larsen et al., 2005). In addition, and just underneath the PS capsule, there is a rigid structure called the cell wall. It is considered to be the primary determinant of *C. neoformans* resistance to stress and environmental aggressions. The cell wall architecture, thoroughly described in the introduction of the present study, consists mainly of a polymer network, including chitin, glucans, manans and galactomanans as its major components (Roncero, 2002; Ruiz-Herrera et al., 2002).

Polarized cell growth (PCG) and directional cell division (DCD) are fundamental and essential processes for the development of eukaryotes. PCG involves asymmetric growth of a cell region to form specific cell structures or shapes. The resulting specialized structures are critical for the function of several cell types and can help mediate various cell interactions during development. Some examples are the absorption of nutrients by epithelial cell microvilli (Mooseker, 1985) and the interaction between T and B cells (Kupfer et al., 1986; Madden and Snyder, 1998). Likewise, PCG in fungi occurs by inserting new material into the plasma membrane via the secretory pathways together with concomitant cell wall remodeling. It can be either triggered by internal factors, for example progression of the cell cycle, or by external factors, such as changes in the environment or nutritional status (Bassilana et al., 2020). Although filamentous fungi and yeasts show obvious differences in their growth modes, they share three basic properties that allow for PCG and the formation of a diverse variety of cellular forms: **(I)** symmetry breaking, in which an initially isotropic cell generates a polarized growth axis, **(II)** maintenance of polarity, which refers to the stabilization of the polarity axis, so that polar growth is maintained, and finally **(III)** depolarization, in which polarity is lost in a controlled manner. The balance between polarity maintenance and depolarization generates the diversity in fungal cell forms (Lin et al., 2014). Fungal cells are not always polarized during the early stages of development. They usually undergo an initial period of non-polar isotropic expansion (for example, spores from yeast stem cells). Ultimately, however, cell symmetry must be broken, and a polarity axis generated, both for the selection of the sprouting site or for the development of polar structures, such as hyphae.

Many of the studies that focused on cell division events for pathogenic yeasts used paradigms established in the ascomycete *Saccharomyces cerevisiae*. However, basidiomycete yeasts, such as *C. neoformans,* show conserved and distinct features in their morphogenesis. It only produces hyphae during sexual differentiation (Lin et al., 2014) and their produced spores are quite infectious and can be the primary particle inhaled during a natural infection (Giles et al., 2009; Velagapudi et al., 2009). Once inhaled, upon reaching the lungs, the Cryptococci spores germinate to produce yeast cells. In the context of infection, this fungus grows within the human host almost exclusively in the form of yeasts. Histopathological studies have shown that hyphal forms are rarely found during human infections by *C. neoformans*. and elongated fungal morphologies are only observed as rare variants among clinical strains (Baker and Haugen, 1955; Fu et al., 2019; Shadomy and Utz, 1966).

Cellular events during *C. neoformans* yeast cell morphogenesis are well described, but still lack information regarding ultrastructural changes. In general, cells undergo a cell division cycle with asexual and repeated clonal budding of a haploid yeast cell; however, unlike *S. cerevisiae*, in which subsequent sprouting events occur adjacent to previous scars, *C. neoformans* preferentially and repeatedly generates their daughter cells from the same location, as shown in the present study. For this reason, scar count, as a result of budding, is unlikely to provide an accurate age measurement of cryptococcal cells (Adams, 2004; Zhao et al., 2019).

The fungal cell wall is a protective barrier that resists environmental and osmotic stresses, maintaining cell morphology and regulating membrane permeability, as well as a wide range of essential roles during the fungus's interaction with its environment (Free, 2013; Gooday, 1995). However, in spite of serving as a protective structure, the cell wall also needs to be remodeled and even partially ruptured for the subsequent budding events that will allow the perpetuation of the fungus in its chosen infection site. Our results not only corroborate this hypothesis but also describe for the first time, to the best of our knowledge, the morphological features of how this remodeling occurs. We showed that the cell wall starts to form a fissure-like structure that culminates with the opening of a specialized region where *C. neoformans* preferentially and repeatedly generates its daughter cells. The cell wall is then reorganized into layers similar to “wafer cookies” around the specialized region. We conjecture that the formation of this region is related to a protruding force coming from inside the cell.

However, apart from the mechanical aspect, we cannot completely rule out the possibility of a change in biochemical composition to facilitate this process. It is known that the cell wall is divided into two layers with specific components. The inner layer is mainly composed of β-glucan and chitin arranged as fibers parallel to the plasma membrane and the outer layer contains α-glucan and β-glucan (O’Meara and Alspaugh, 2012; Sakaguchi et al., 1993). Moreover, several cell wall proteins have been described to have key roles in the capsule architecture. Some of these proteins, such as the GPI-linked β-glucanase Gas1, have been implicated in remodeling of the cell wall as it directly acts on β-1,3-glucans (Eigenheer et al., 2007; Levitz and Specht, 2006). Therefore, preceding cell budding, perhaps still during the PCG stage, the structural components of the cell wall may be reorganized in order to form a region where budding is facilitated. In the present study, we have described the morphological aspects of the cell wall

remodeling. The molecular and mechanical details constitute lines of investigation for future studies.

Beyond the cell wall and attached to its surface lies the PS capsule. Despite its homogeneous appearance, when viewed through light microscopy, several lines of evidence show that the capsule is a highly heterogeneous structure with a complex and dynamic spatial organization. It is known, for example, that the capsule matrix exhibits clear vertical stratification, with distinct density regions, with its inner part having a higher fiber density than its outer region (Araújo et al., 2016, 2017; Bryan et al., 2005; S. Frases et al., 2009; Gates et al., 2004). Although softer than the cell wall and presenting viscoelastic behavior (Araújo et al., 2019; Susana Frases et al., 2009), the high PS density of the inner region prevents the penetration of larger macromolecules, including antibodies and proteins of the complement system, restricting the access of these molecules to the cell wall (Gates et al., 2004; Gates and Kozel, 2006). Therefore, one could speculate that the capsule might also undergo remodeling during budding. Indeed, our results show that the PSs constituting the capsule undergo shape changes around the specialized budding region. The change in shape seems to be correlated with the conjectured protruding force, as the capsule fibers tend to orient towards the budding event. Finally, our results also demonstrate that the PS capsule works as a protective shield around the specialized region during the budding event.

In conclusion, we have combined the state-of-the-art in light and electron microscopy techniques to describe the structural changes that synergistically occur between the capsule, cell wall and plasma membrane during the budding phenomenon in *C. neoformans*. We have presented evidences supporting a possible remodeling through mechanical protruding forces originated inside the yeast cell, although the magnitude of such force and the mechanism behind its generation have yet to be elucidated. All morphological changes observed, particularly those from the cell wall, act together and create a specialized region with characteristics that seem to favor budding events, which is able to partially explain why budding in *C. neoformans* always occur in the same region. However, the complete mechanism may also involve controlled rearrangement of the molecules that constitute both the cell wall and the PS capsule and will be explored in future studies. We also aim to explore and characterize further these specialized regions such that they could be used as potential drug-targets against cryptococcosis.

## 5. Author Contributions

**Glauber R. de S. Araújo:** Conceptualization, Methodology, Investigation, Visualization, Data curation, Formal analysis, Writing - original draft, Writing - review & editing.

**Carolina de L. Alcantara:** Methodology, Writing - review & editing

**Noêmia Rodrigues:** Methodology, Writing - review & editing

**Wanderley de Souza:** Supervision, Funding acquisition, Formal analysis, Writing - review & editing

**Bruno Pontes:** Conceptualization, Methodology, Investigation, Visualization, Data curation, Resources, Supervision, Funding acquisition, Formal analysis, Writing - original draft, Writing - review & editing.

**Susana Frases:** Conceptualization, Methodology, Investigation, Visualization, Data curation, Resources, Supervision, Funding acquisition, Formal analysis, Writing - original draft, Writing - review & editing.

## 6. Conflict of interest

The authors declare that they have no known competing financial interests or personal relationships that could have appeared to influence the work reported in this paper.

## 7. Acknowledgments

We acknowledge Dr. Barbara Hissa for critical reading and scientific editing of the manuscript. We also thank the technicians from Centro Nacional de Biologia Estrutural e Bioimagem (CENABIO/UFRJ) for all-important help. This work was supported by the Brazilian agencies Conselho Nacional de Desenvolvimento Científico e Tecnológico (CNPq), Coordenação de Aperfeiçoamento de Pessoal de Nível Superior (CAPES) - Finance Code 001 and Fundação Carlos Chagas Filho de Amparo à Pesquisa do Estado do Rio de Janeiro (FAPERJ).

## 8. Appendix A. Supplementary data

Supplementary video 1, Supplementary video 2 and Supplementary video 3.

## 8. References

Abràmoff, M.D., Magalhaes, P.., Ram, S.J., 2004. Image processing with ImageJ. Biophotonics Int. 11, 36–42.

Adams, D.J., 2004. Fungal cell wall chitinases and glucanases. Microbiology 150, 2029–

2035. https://doi.org/10.1099/mic.0.26980-0

Albuquerque, P., Nicola, A.M., Magnabosco, D.A.G., Derengowski, L. da S., Crisóstomo, L.S., Xavier, L.C.G., Frazão, S. de O., Guilhelmelli, F., de Oliveira, M.A., Dias, J. do N., Hurtado, F.A., Teixeira, M. de M., Guimarães, A.J., Paes, H.C., Bagagli, E., Felipe, M.S.S., Casadevall, A., Silva-Pereira, I., 2019. A hidden battle in the dirt: Soil amoebae interactions with Paracoccidioides spp. PLoS Negl. Trop. Dis. 13, e0007742. https://doi.org/10.1371/journal.pntd.0007742

Araújo, G.R. de S., Freitas, G.J.C., Fonseca, F.L., Leite, P.E.C., Rocha, G.M., de Souza, W., Santos, D.A., Frases, S., 2017. The environmental yeast Cryptococcus liquefaciens produces capsular and secreted polysaccharides with similar pathogenic properties to those of C. neoformans. Sci. Rep. 7, 46768. https://doi.org/10.1038/srep46768

Araújo, G.R., Fontes, G.N., Leão, D., Rocha, G.M., Pontes, B., Sant'Anna, C., de Souza, W., Frases, S., 2016. Cryptococcus neoformans capsular polysaccharides form branched and complex filamentous networks viewed by high-resolution microscopy. J. Struct. Biol. 193, 75–82. https://doi.org/10.1016/j.jsb.2015.11.010

Araújo, G.R.D. de S., Viana, N.B., Pontes, B., Frases, S., 2019. Rheological properties of cryptococcal polysaccharide change with fiber size, antibody binding and temperature. Future Microbiol. 14, 867–884. https://doi.org/10.2217/fmb-2018-0320

Araujo, G.S., Fonseca, F.L., Pontes, B., Torres, A., Cordero, R.J.B., Zancopé-Oliveira, R.M., Casadevall, A., Viana, N.B., Nimrichter, L., Rodrigues, M.L., Garcia, E.S., de Souza, W., Frases, S., 2012. Capsules from pathogenic and non-pathogenic Cryptococcus spp. manifest significant differences in structure and ability to protect against phagocytic cells. PLoS One 7. https://doi.org/10.1371/journal.pone.0029561

Baker, L.G., Specht, C.A., Lodge, J.K., 2011. Cell wall chitosan is necessary for virulence in the opportunistic pathogen Cryptococcus neoformans. Eukaryot. Cell 10, 1264–1268. https://doi.org/10.1128/EC.05138-11

Baker, R.D., Haugen, R.K., 1955. Tissue changes and tissue diagnosis in Cryptococcosis: A study of 26 cases. Am. J. Clin. Pathol. 25, 14–24. https://doi.org/10.1093/ajcp/25.1.14

Banks, I.R., Specht, C.A., Donlin, M.J., Gerik, K.J., Levitz, S.M., Lodge, J.K., 2005. A chitin synthase and its regulator protein are critical for chitosan production and growth of the fungal pathogen Cryptococcus neoformans. Eukaryot. Cell 4, 1902–

1912. https://doi.org/10.1128/EC.4.11.1902-1912.2005

Bassilana, M., Puerner, C., Arkowitz, R.A., 2020. External signal–mediated polarized growth in fungi. Curr. Opin. Cell Biol. 62, 150–158. https://doi.org/10.1016/j.ceb.2019.11.001

Benchimol, M., Goncalves, N.R., de Souza, W., 1993. Rapid primary microwave-glutaraldehyde fixation preserves the plasma membrane and intracellular structures of the protozoan Tritrichomonas foetus. Microsc. Res. Tech. 25, 286–290. https://doi.org/10.1002/jemt.1070250404

Bose, I., Reese, A.J., Ory, J.J., Janbon, G., Doering, T.L., 2003. A yeast under Cover: the capsule of Cryptococcus neoformans. Eukaryot. Cell 2, 655–663. https://doi.org/10.1128/EC.2.4.655-663.2003

Boudaoud, A., Burian, A., Borowska-Wykręt, D., Uyttewaal, M., Wrzalik, R., Kwiatkowska, D., Hamant, O., 2014. FibrilTool, an ImageJ plug-in to quantify fibrillar structures in raw microscopy images. Nat. Protoc. 9, 457–63. https://doi.org/10.1038/nprot.2014.024

Bryan, R.A., Zaragoza, O., Zhang, T., Ortiz, G., Casadevall, A., Dadachova, E., 2005. Radiological studies reveal radial differences in the architecture of the polysaccharide capsule of Cryptococcus neoformans. Eukaryot. Cell 4, 465–475. https://doi.org/10.1128/EC.4.2.465-475.2005

Casadevall, A., Perfect, J.R., 2008. Cryptococcus neoformans, in: Medical Mycology. pp. 371–371. https://doi.org/10.1111/j.1365-280X.1999.00238.x

Casadevall, A., Pirofski, L., 2007. Accidental virulence, cryptic pathogenesis, martians, lost hosts, and the pathogenicity of environmental microbes. Eukaryot. Cell 6, 2169–74. https://doi.org/10.1128/EC.00308-07

Cox, G.M., Harrison, T.S., McDade, H.C., Taborda, C.P., Heinrich, G., Casadevall, A., Perfect, J.R., 2003. Superoxide dismutase influences the virulence of Cryptococcus neoformans by affecting growth within macrophages. Infect. Immun. 71, 173–80. https://doi.org/10.1128/iai.71.1.173-180.2003

Cox, G.M., McDade, H.C., Chen, S.C., Tucker, S.C., Gottfredsson, M., Wright, L.C., Sorrell, T.C., Leidich, S.D., Casadevall, A., Ghannoum, M.A., Perfect, J.R., 2001. Extracellular phospholipase activity is a virulence factor for Cryptococcus neoformans. Mol. Microbiol. 39, 166–75. https://doi.org/10.1046/j.1365-2958.2001.02236.x

Cox, G.M., Mukherjee, J., Cole, G.T., Casadevall, A., Perfect, J.R., 2000. Urease as a

virulence factor in experimental cryptococcosis. Infect. Immun. 68, 443–448. https://doi.org/10.1128/IAI.68.2.443-448.2000

Doering, T.L., 2000. How does Cryptococcus get its coat? Trends Microbiol. https://doi.org/10.1016/S0966-842X(00)01890-4

Doering, T.L., Nosanchuk, J.D., Roberts, W.K., Casadevall, A., 1999. Melanin as a potential cryptococcal defence against microbicidal proteins. Med. Mycol. 37, 175–181. https://doi.org/10.1046/j.1365-280X.1999.00218.x

Dong, Z.M., Murphy, J.W., Zhao Ming Dong, Murphy, J.W., 1995. Effects of the two varieties of Cryptococcus neoformans cells and culture filtrate antigens on neutrophil locomotion. Infect. Immun. 63, 2632–44.

Eigenheer, R.A., Jin Lee, Y., Blumwald, E., Phinney, B.S., Gelli, A., 2007. Extracellular glycosylphosphatidylinositol-anchored mannoproteins and proteases of Cryptococcus neoformans. FEMS Yeast Res. 7, 499–510. https://doi.org/10.1111/j.1567-1364.2006.00198.x

Ellis, D.H., Pfeiffer, T.J., 1990. Ecology, life cycle, and infectious propagule of Cryptococcus neoformans. Lancet (London, England) 336, 923–5. https://doi.org/10.1016/0140-6736(90)92283-n

Faganello, J., Arruda, W., Schrank, A., Vainstein, M.H., 2006. An alternative method to prepare samples of the pathogenic yeast Cryptococcus neoformans for scanning electron microscopy analysis. J. Microbiol. Methods 64, 416–419. https://doi.org/10.1016/j.mimet.2005.07.003

Feldmesser, M., Kress, Y., Casadevall, A., 2001. Dynamic changes in the morphology of Cryptococcus neoformans during murine pulmonary infection. Microbiology 147, 2355–2365. https://doi.org/10.1099/00221287-147-8-2355

Fonseca, F.L., Guimarães, A.J., Kmetzsch, L., Dutra, F.F., Silva, F.D., Taborda, C.P., Araujo, G. de S., Frases, S., Staats, C.C., Bozza, M.T., Schrank, A., Vainstein, M.H., Nimrichter, L., Casadevall, A., Rodrigues, M.L., 2013. Binding of the wheat germ lectin to Cryptococcus neoformans chitooligomers affects multiple mechanisms required for fungal pathogenesis. Fungal Genet. Biol. 60, 64–73. https://doi.org/10.1016/j.fgb.2013.04.005

Frases, Susana, Pontes, B., Nimrichter, L., Rodrigues, M.L., Viana, N.B., Casadevall, A., 2009. The elastic properties of the Cryptococcus neoformans capsule. Biophys. J. 97, 937–945. https://doi.org/10.1016/j.bpj.2009.04.043

Frases, S., Pontes, B., Nimrichter, L., Viana, N.B., Rodrigues, M.L., Casadevall, A.,

615 2009. Capsule of Cryptococcus neoformans grows by enlargement of
616 polysaccharide molecules. Proc. Natl. Acad. Sci. 106, 1228–1233.
617 https://doi.org/10.1073/pnas.0808995106
618 Free, S.J., 2013. Fungal cell wall organization and biosynthesis. Adv. Genet. 81, 33–82.
619 https://doi.org/10.1016/B978-0-12-407677-8.00002-6
620 Fries, B.C., Taborda, C.P., Serfass, E., Casadevall, A., 2001. Phenotypic switching of
621 Cryptococcus neoformans occurs in vivo and influences the outcome of infection. J.
622 Clin. Invest. 108, 1639–1648. https://doi.org/10.1172/JCI13407
623 Fu, C., Thielhelm, T.P., Heitman, J., 2019. Unisexual reproduction promotes competition
624 for mating partners in the global human fungal pathogen Cryptococcus
625 deneoformans. PLOS Genet. 15, e1008394.
626 https://doi.org/10.1371/journal.pgen.1008394
627 Gates, M.A., Kozel, T.R., 2006. Differential localization of complement component 3
628 within the capsular matrix of Cryptococcus neoformans. Infect. Immun. 74, 3096–
629 3106. https://doi.org/10.1128/IAI.01213-05
630 Gates, M.A., Thorkildson, P., Kozel, T.R., 2004. Molecular architecture of the
631 Cryptococcus neoformans capsule. Mol. Microbiol. 52, 13–24.
632 https://doi.org/10.1111/j.1365-2958.2003.03957.x
633 Giberson, R.T., Austin, R.L., Charlesworth, J., Adamson, G., Herrera, G.A., 2003.
634 Microwave and digital imaging technology reduce turnaround times for diagnostic
635 electron microscopy. Ultrastruct. Pathol. 27, 187–196.
636 https://doi.org/10.1080/01913120309937
637 Giles, S.S., Dagenais, T.R.T., Botts, M.R., Keller, N.P., Hull, C.M., 2009. Elucidating
638 the pathogenesis of spores from the human fungal pathogen Cryptococcus
639 neoformans. Infect. Immun. 77, 3491–3500. https://doi.org/10.1128/IAI.00334-09
640 Goldman, D.L., Fries, B.C., Franzot, S.P., Montella, L., Casadevall, A., 1998. Phenotypic
641 switching in the human pathogenic fungus Cryptococcus neoformans is associated
642 with changes in virulence and pulmonary inflammatory response in rodents. Proc.
643 Natl. Acad. Sci. U. S. A. 95, 14967–72. https://doi.org/10.1073/pnas.95.25.14967
644 Goldman, J.D., Vollmer, M.E., Luks, A.M., 2010. Cryptococcosis in the
645 immunocompetent patient. Respir. Care 55, 1499–503.
646 Gómez, B.L., Nosanchuk, J.D., 2003. Melanin and fungi. Curr. Opin. Infect. Dis. 16, 91–
647 6. https://doi.org/10.1097/00001432-200304000-00005
648 Gooday, G.W., 1995. The growing fungus. Springer US.

649 Henao-Martínez, A.F., Beckham, J.D., 2015. Cryptococcosis in solid organ transplant
650 recipients. Curr. Opin. Infect. Dis. 28, 300–7.
651 https://doi.org/10.1097/QCO.0000000000000171
652 Huffnagle, G.B., Chen, G.-H., Curtis, J.L., McDonald, R.A., Strieter, R.M., Toews, G.B.,
653 1995. Down-regulation of the afferent phase of T cell-mediated pulmonary
654 inflammation and immunity by a high melanin-producing strain of Cryptococcus
655 neoformans. J. Immunol.
656 James, P.G., Cherniak, R., Jones, R.G., Stortz, C.A., Reiss, E., 1990. Cell-wall glucans
657 of Cryptococcus neoformans CAP 67. Carbohydr. Res. 198, 23–38.
658 https://doi.org/10.1016/0008-6215(90)84273-W
659 Kozel, T.R., Gulley, W.F., Cazin, J., 1977. Immune response to Cryptococcus
660 neoformans soluble polysaccharide: Immunological unresponsiveness. Infect.
661 Immun. 18, 701–707.
662 Kremer, J.R., Mastronarde, D.N., McIntosh, J.R., 1996. Computer Visualization of
663 Three-Dimensional Image Data Using IMOD. J. Struct. Biol. 116, 71–76.
664 https://doi.org/10.1006/jsbi.1996.0013
665 Kupfer, A., Swain, S.L., Janeway, C.A., Singer, S.J., 1986. The specific direct interaction
666 of helper T cells and antigen-presenting B cells. Proc. Natl. Acad. Sci. 83, 6080–
667 6083. https://doi.org/10.1073/pnas.83.16.6080
668 Larsen, R.A., Pappas, P.G., Perfect, J., Aberg, J.A., Casadevall, A., Cloud, G.A., James,
669 R., Filler, S., Dismukes, W.E., 2005. Phase I evaluation of the safety and
670 pharmacokinetics of murine-derived anticryptococcal antibody 18B7 in subjects
671 with treated cryptococcal meningitis. Antimicrob. Agents Chemother. 49, 952–958.
672 https://doi.org/10.1128/AAC.49.3.952-958.2005
673 Lee, D.-J., Bahn, Y.-S., Kim, H.-J., Chung, S.-Y., Kang, H.A., 2015. Unraveling the novel
674 structure and biosynthetic pathway of O-linked glycans in the Golgi apparatus of the
675 human pathogenic yeast Cryptococcus neoformans. J. Biol. Chem. 290, 1861–73.
676 https://doi.org/10.1074/jbc.M114.607705
677 Levitz, S.M., Specht, C.A., 2006. The molecular basis for the immunogenicity of
678 *Cryptococcus neoformans* mannoproteins. FEMS Yeast Res. 6, 513–524.
679 https://doi.org/10.1111/j.1567-1364.2006.00071.x
680 Liao, T.-L., Chen, Y.-M., Chen, D.-Y., 2016. Risk factors for cryptococcal infection
681 among patients with rheumatoid arthritis receiving different immunosuppressive
682 medications. Clin. Microbiol. Infect. 22, 815.e1-815.e3.

683 https://doi.org/10.1016/j.cmi.2016.05.030
684 Lin, X., Alspaugh, J.A., Liu, H., Harris, S., 2014. Fungal morphogenesis. Cold Spring
685 Harb. Perspect. Med. 5, a019679. https://doi.org/10.1101/cshperspect.a019679
686 Liu, L., Tewari, R.P., Williamson, P.R., 1999. Laccase protects Cryptococcus
687 neoformans from antifungal activity of alveolar macrophages. Infect. Immun. 67,
688 6034–9.
689 Macher, A.M., Bennett, J.E., Gadek, J.E., Frank, M.M., 1978. Complement depletion in
690 cryptococcal sepsis. J. Immunol. 120, 1686–1690.
691 Madden, K., Snyder, M., 1998. Cell polarity and morphogenesis in budding yeast. Annu.
692 Rev. Microbiol. 52, 687–744. https://doi.org/10.1146/annurev.micro.52.1.687
693 Manners, D.J., Masson, A.J., Patterson, J.C., Björndal, H., Lindberg, B., 1973. The
694 structure of a beta-(1-6)-D-glucan from yeast cell walls. Biochem. J. 135, 31–6.
695 https://doi.org/10.1042/bj1350031
696 Mastronarde, D.N., 1997. Dual-Axis tomography: An Approach with Alignment
697 Methods That Preserve Resolution. J. Struct. Biol. 120, 343–352.
698 https://doi.org/10.1006/jsbi.1997.3919
699 McFadden, D., Zaragoza, O., Casadevall, A., 2006. The capsular dynamics of
700 Cryptococcus neoformans. Trends Microbiol. 14, 497–505.
701 https://doi.org/10.1016/j.tim.2006.09.003
702 McFadden, D.C., De Jesus, M., Casadevall, A., 2006. The physical properties of the
703 capsular polysaccharides from Cryptococcus neoformans suggest features for
704 capsule construction. J. Biol. Chem. 281, 1868–1875.
705 https://doi.org/10.1074/jbc.M509465200
706 Mitchell, D.H., Sorrell, T.C., Allworth, A.M., Heath, C.H., McGregor, A.R., Papanaoum,
707 K., Richards, M.J., Gottlieb, T., 1995. Cryptococcal disease of the CNS in
708 immunocompetent hosts: influence of cryptococcal variety on clinical
709 manifestations and outcome. Clin. Infect. Dis. 20, 611–6.
710 https://doi.org/10.1093/clinids/20.3.611
711 Mooseker, M.S., 1985. Organization, chemistry, and assembly of the cytoskeletal
712 apparatus of the intestinal brush border. Annu. Rev. Cell Biol. 1, 209–41.
713 https://doi.org/10.1146/annurev.cb.01.110185.001233
714 Murakami, T., Iida, N., Taguchi, T., Ohtani, O., Kikuta, A., Ohtsuka, A., Itoshima, T.,
715 1983. Conductive staining of biological specimens for scanning electron microscopy
716 with special reference to ligand-mediated osmium impregnation. Scan. Electron

717 Microsc. 235–46.
718 Murphy, J.W., Cozad, G.C., 1972. Immunological unresponsiveness induced by
719 cryptococcal capsular polysaccharide assayed by the hemolytic plaque technique.
720 Infect. Immun. 5, 896–901.
721 O'Meara, T.R., Alspaugh, J.A., 2012. The Cryptococcus neoformans capsule: a sword
722 and a shield. Clin. Microbiol. Rev. 25, 387–408.
723 https://doi.org/10.1128/CMR.00001-12
724 Okagaki, L.H., Strain, A.K., Nielsen, J.N., Charlier, C., Baltes, N.J., Chrétien, F.,
725 Heitman, J., Dromer, F., Nielsen, K., 2010. Cryptococcal cell morphology affects
726 host cell interactions and pathogenicity. PLoS Pathog. 6, e1000953.
727 https://doi.org/10.1371/journal.ppat.1000953
728 Park, B.J., Wannemuehler, K.A., Marston, B.J., Govender, N., Pappas, P.G., Chiller,
729 T.M., 2009. Estimation of the current global burden of cryptococcal meningitis
730 among persons living with HIV/AIDS. AIDS 23, 525–30.
731 https://doi.org/10.1097/QAD.0b013e328322ffac
732 Park, J.-N., Lee, D.-J., Kwon, O., Oh, D.-B., Bahn, Y.-S., Kang, H.A., 2012. Unraveling
733 unique structure and biosynthesis pathway of N-linked glycans in human fungal
734 pathogen Cryptococcus neoformans by glycomics analysis. J. Biol. Chem. 287,
735 19501–15. https://doi.org/10.1074/jbc.M112.354209
736 Perfect, J.R., 2013. Fungal diagnosis: how do we do it and can we do better? Curr. Med.
737 Res. Opin. 29 Suppl 4, 3–11. https://doi.org/10.1185/03007995.2012.761134
738 Perfect, J.R., Casadevall, A., 2011. Cryptococcus. American Society of Microbiology.
739 https://doi.org/10.1128/9781555816858
740 Pontes, B., Frases, S., 2015. The Cryptococcus neoformans capsule: Lessons from the use
741 of optical tweezers and other biophysical tools. Front. Microbiol. 6, 640.
742 https://doi.org/10.3389/fmicb.2015.00640
743 Reese, A.J., Doering, T.L., 2003. Cell wall α-1,3-glucan is required to anchor the
744 Cryptococcus neoformans capsule. Mol. Microbiol. 50, 1401–1409.
745 https://doi.org/10.1046/j.1365-2958.2003.03780.x
746 Reilly, M.C., Aoki, K., Wang, Z.A., Skowyra, M.L., Williams, M., Tiemeyer, M.,
747 Doering, T.L., 2011. A xylosylphosphotransferase of Cryptococcus neoformans acts
748 in protein O-glycan synthesis. J. Biol. Chem. 286, 26888–99.
749 https://doi.org/10.1074/jbc.M111.262162
750 Retini, C., Vecchiarelli, A., Monari, C., Bistoni, F., Kozel, T.R., 1998. Encapsulation of

751 Cryptococcus neoformans with glucuronoxylomannan inhibits the antigen-
752 presenting capacity of monocytes. Infect. Immun. 66, 664–9.
753 Rodrigues, M.L., Dobroff, A.S.S., Couceiro, J.N. dos S.S., Alviano, C.S., Schauer, R.,
754 Travassos, L.R., 2002. Sialylglycoconjugates and sialyltransferase activity in the
755 fungus Cryptococcus neoformans. Glycoconj. J. 19, 165–73.
756 https://doi.org/10.1023/A:1024245606607
757 Rodrigues, M.L., Fonseca, F.L., Frases, S., Casadevall, A., Nimrichter, L., 2009. The still
758 obscure attributes of cryptococcal glucuronoxylomannan. Med. Mycol. 47, 783–8.
759 https://doi.org/10.3109/13693780902788621
760 Rodrigues, M.L., Nimrichter, L., Oliveira, D.L., Frases, S., Miranda, K., Zaragoza, O.,
761 Alvarez, M., Nakouzi, A., Feldmesser, M., Casadevall, A., 2007. Vesicular
762 polysaccharide export in Cryptococcus neoformans is a eukaryotic solution to the
763 problem of fungal trans-cell wall transport. Eukaryot. Cell 6, 48–59.
764 https://doi.org/10.1128/EC.00318-06
765 Roncero, C., 2002. The genetic complexity of chitin synthesis in fungi. Curr. Genet. 41,
766 367–78. https://doi.org/10.1007/s00294-002-0318-7
767 Ruiz-Herrera, J., González-Prieto, J.M., Ruiz-Medrano, R., 2002. Evolution and
768 phylogenetic relationships of chitin synthases from yeasts and fungi. FEMS Yeast
769 Res. 1, 247–56. https://doi.org/10.1111/j.1567-1364.2002.tb00042.x
770 Sakaguchi, N., Baba, T., Fukuzawa, M., Ohno, S., 1993. Ultrastructural study of
771 Cryptococcus neoformans by quick-freezing and deep-etching method.
772 Mycopathologia 121, 133–141. https://doi.org/10.1007/BF01104068
773 Schneider, C.A., Rasband, W.S., Eliceiri, K.W., 2012. NIH image to ImageJ: 25 years of
774 image analysis. Nat. Methods 9, 671–675. https://doi.org/10.1038/nmeth.2089
775 Seligman, A.M., Wasserkrug, H.L., Hanker, J.S., 1966. A new staining method (OTO)
776 for enhancing contrast of lipid-containing membranes and droplets in osmium
777 tetroxide-fixed tissue with osmiophilic thiocarbohydrazide (TCH). J. Cell Biol. 30,
778 424–32. https://doi.org/10.1083/jcb.30.2.424
779 Shadomy, H.J., Utz, J.P., 1966. Preliminary studies on a hyphaforming mutant of
780 Cryptococcus neoformans. Mycologia 58, 383–90.
781 Singh, N., Dromer, F., Perfect, J.R., Lortholary, O., 2008. Cryptococcosis in solid organ
782 transplant recipients: current state of the science. Clin. Infect. Dis. 47, 1321–7.
783 https://doi.org/10.1086/592690
784 Trevijano-Contador, N., de Oliveira, H.C., García-Rodas, R., Rossi, S.A., Llorente, I.,

785 Zaballos, Á., Janbon, G., Ariño, J., Zaragoza, Ó., 2018. Cryptococcus neoformans
786 can form titan-like cells in vitro in response to multiple signals. PLoS Pathog. 14,
787 e1007007. https://doi.org/10.1371/journal.ppat.1007007
788 Velagapudi, R., Hsueh, Y.-P., Geunes-Boyer, S., Wright, J.R., Heitman, J., 2009. Spores
789 as infectious propagules of Cryptococcus neoformans. Infect. Immun. 77, 4345–55.
790 https://doi.org/10.1128/IAI.00542-09
791 Wang, Y., Aisen, P., Casadevall, A., 1995. Cryptococcus neoformans melanin and
792 virulence: mechanism of action. Infect. Immun. 63, 3131–6.
793 Wang, Z.A., Li, L.X., Doering, T.L., 2018. Unraveling synthesis of the cryptococcal cell
794 wall and capsule. Glycobiology 28, 719–730.
795 https://doi.org/10.1093/glycob/cwy030
796 Willingham, M.C., Rutherford, A. V, 1984. The use of Osmium-Thiocarbohydrazide-
797 Osmium (OTO) and ferrocyanide-reduced osmium methods to enhance membrane
798 contrast and preservation in cultured cells. J. Histochem. Cytochem. 32, 455–460.
799 https://doi.org/10.1177/32.4.6323574
800 Zaragoza, O., 2019. Basic principles of the virulence of Cryptococcus. Virulence 10, 490–
801 501. https://doi.org/10.1080/21505594.2019.1614383
802 Zaragoza, O., Chrisman, C.J., Castelli, M.V., Frases, S., Cuenca-Estrella, M., Rodríguez-
803 Tudela, J.L., Casadevall, A., 2008. Capsule enlargement in Cryptococcus
804 neoformans confers resistance to oxidative stress suggesting a mechanism for
805 intracellular survival. Cell. Microbiol. 10, 2043–57. https://doi.org/10.1111/j.1462-
806 5822.2008.01186.x
807 Zaragoza, O., Fries, B.C., Casadevall, A., 2003. Induction of capsule growth in
808 Cryptococcus neoformans by mammalian serum and CO(2). Infect. Immun. 71,
809 6155–64. https://doi.org/10.1128/iai.71.11.6155-6164.2003
810 Zaragoza, O., McClelland, E.E., Telzak, A., Casadevall, A., 2006a. Equatorial ring-like
811 channels in the Cryptococcus neoformans polysaccharide capsule. FEMS Yeast Res.
812 6, 662–6. https://doi.org/10.1111/j.1567-1364.2006.00070.x
813 Zaragoza, O., Nielsen, K., 2013. Titan cells in Cryptococcus neoformans: cells with a
814 giant impact. Curr. Opin. Microbiol. 16, 409–13.
815 https://doi.org/10.1016/j.mib.2013.03.006
816 Zaragoza, O., Rodrigues, M.L., De Jesus, M., Frases, S., Dadachova, E., Casadevall, A.,
817 2009. The capsule of the fungal pathogen Cryptococcus neoformans. Adv. Appl.
818 Microbiol. 68, 133–216. https://doi.org/10.1016/S0065-2164(09)01204-0

819 Zaragoza, O., Telzak, A., Bryan, R.A., Dadachova, E., Casadevall, A., 2006b. The
820 polysaccharide capsule of the pathogenic fungus Cryptococcus neoformans enlarges
821 by distal growth and is rearranged during budding. Mol. Microbiol. 59, 67–83.
822 https://doi.org/10.1111/j.1365-2958.2005.04928.x
823 Zhao, Y., Lin, J., Fan, Y., Lin, X., 2019. Life cycle of Cryptococcus neoformans. Annu.
824 Rev. Microbiol. 73, 17–42. https://doi.org/10.1146/annurev-micro-020518-120210
825
826
827 **9. Figure Legends**
828
829 **Figure 1: Selected images from a video microscopy movie of *C. neoformans,* grown**
830 **in Sabouraud medium, showing budding evolution**. A-D) Snapshots taken at 0,
831 1h07min, 02h12min and 03h21min, respectively, showing how the budding events evolve
832 with time. Green arrowheads indicate yeasts during the division process that takes
833 approximately (1.3 ± 0.3) h / cell. They also show that daughter cells always bud
834 unipolarly and repeatedly from the same cell region. G1 indicates first generation cells,
835 G1.1 daughter cell from the first generation, the other numbers follow a similar logic.
836 Scale bar is 5 μm. (Supplementary video 1).
837
838 **Figure 2: Conventional fluorescence microscopy images of *C. neoformans* stained**
839 **with Uvitex2D depicting chitin polymers at the cell wall. A)** Fixed and stained *C.*
840 *neoformans* with chitin labeled in blue. Notice the discontinuity of the cell wall staining
841 (red arrow). Those are the specialized regions (SR) in yeasts. **B)** Grey scale image of A.
842 C1, C2 and C3 are cells that are under different budding stages (see red arrows). **C)** Zoom
843 of C1, C2 and C3 (upper panel) with their respective 3D surface plots (lower panel).
844 Surface plots indicate that the cell walls in SRs have a lower fluorescence intensity when
845 compared to the entire cell wall rims. Scale bars are all 10 μm.
846
847 **Figure 3: SIM images of *C. neoformans* confirm that both the cell wall and capsule**
848 **deform prior to the budding event and generation of daughter cells.** Yeast cells were
849 fixed and stained for Uvitex2B (blue) and 18B7 antibody (red) so we could follow their
850 walls and PS capsules, respectively, during budding and generation of daughter cells. **A)**
851 2.5D yeast profile, showing that the mother cell (left) has a higher cell wall fluorescence
852 intensity when compared to the daughter cell (right). **B)** 2D representation of the same

853 field as in A. **C)** Representative image of a yeast cell at the beginning of the budding
854 process. SR can be visualized as a discontinuity of the cell wall. **D)** 3D profile of a
855 representative yeast cell also in the beginning of the budding process showing the SR.
856 Scale bars: A 1 μm. B, C and D 2 μm. (Supplementary video 2).
857
858 **Figure 4: Transmission electron microscopy of *C. neoformans* during budding**
859 **reveals that both the cell wall and PS layer reorganize prior to budding.** The right
860 column images (B, C, F) are zoomed images of the panels represented on the left. The
861 green arrowheads indicate the cell wall delamination at different budding stages. **A - B)**
862 Yeast in the beginning of the budding process presents a modest cell wall (CW)
863 delamination in the specialized region (SR). **C - D)** Intermediate cell wall delamination
864 stage and reduction of the PS fiber density at the SR when compared to the rest of the cell
865 perimeter. **E - F)** Discontinuity of the cell wall showing an advanced delamination step
866 in which the cell wall peeling is evident, resembling a "wafer cookie", and the reduction
867 of the density and complexity of the PS fibers around the SR is evident. **LBs:** Lipid
868 Bodies; **CW:** Cell Wall; **PS:** Polysaccharide; **SR:** Specialized region. Scale bars: A, C
869 and E 1 μm ; B, D and F 500 nm.
870
871 **Figure 5: Serial electron tomography and three-dimensional reconstruction of *C.***
872 ***neoformans* show ultrastructural details of the budding process. A – C)** Different z-
873 planes of a serial tomogram of a budding event. The green arrowheads point to the cell
874 wall delamination along different image planes. **D)** Virtual plane of the tomogram where
875 the 3D model was superimposed to highlight the structures that participate and are
876 remodeled in the SR. The upper left cell is the mother cell while the bottom right one is
877 the daughter cell. **E$_{1\text{-}5}$)** Set of sequential slices from the tomogram evidencing the
878 modifications in cell wall cohesion along different angles. Note the presence of a
879 multilamellar membrane and vesicles in synergism with the PSs surrounding the SRs,
880 which probably acts as a shield. **F and G)** Different views of the three-dimensional model
881 from the daughter cell perspective. In **F** we see a front view of the daughter cell wall
882 discontinuity at the region of budding. This region is sealed by several membrane profiles
883 as show in E. In G, a top view of the model where membrane profiles can be seen in
884 between the CW and the cell membrane. Several vesicles (asterisk) could be seen inside
885 the membrane profiles (dark blue) and also between CW and cell membrane (red and

886 brown). **LBs:** Lipid Bodies; **CW:** Cell Wall; **PS:** Polysaccharide; **SR:** Specialized region.
887 Scale bars are all 100 nm. (Supplementary video 3).
888
889 **Figure 6: Scanning electron microscopy images of *C. neoformans* showing the**
890 **alignment of the PS fibers toward the budding region. A - E)** Different examples
891 showing changes in the spatial and conformational orientation of the PS capsule in the
892 SR. Scale bars: A, B and E 2 μm; C and D 5μm. **F)** Plot of the mean anisotropy values of
893 PS fibers around SRs (grey) and outside SRs (black). At least 25 different measurements
894 were performed for each experimental situation. Standard error was used as error bars.
895 **** means $p < 0.0001$ in Student's *t*-test statistics.
896
897
898 **10. Supplementary Material Legends**
899
900 **Supplementary video 1:** Budding phenomena observed in a representative *C.*
901 *neoformans* cell culture (related to Figure 1).
902
903 **Supplementary video 2:** 3D-SIM reconstruction of a representative *C. neoformans* cell
904 in the beginning of the budding process showing the SR (related to Figure 3D).
905
906 **Supplementary video 3:** Set of electron tomography planes showing *C. neoformans*
907 mother and daughter cells during a budding process (related to Figure 5E).

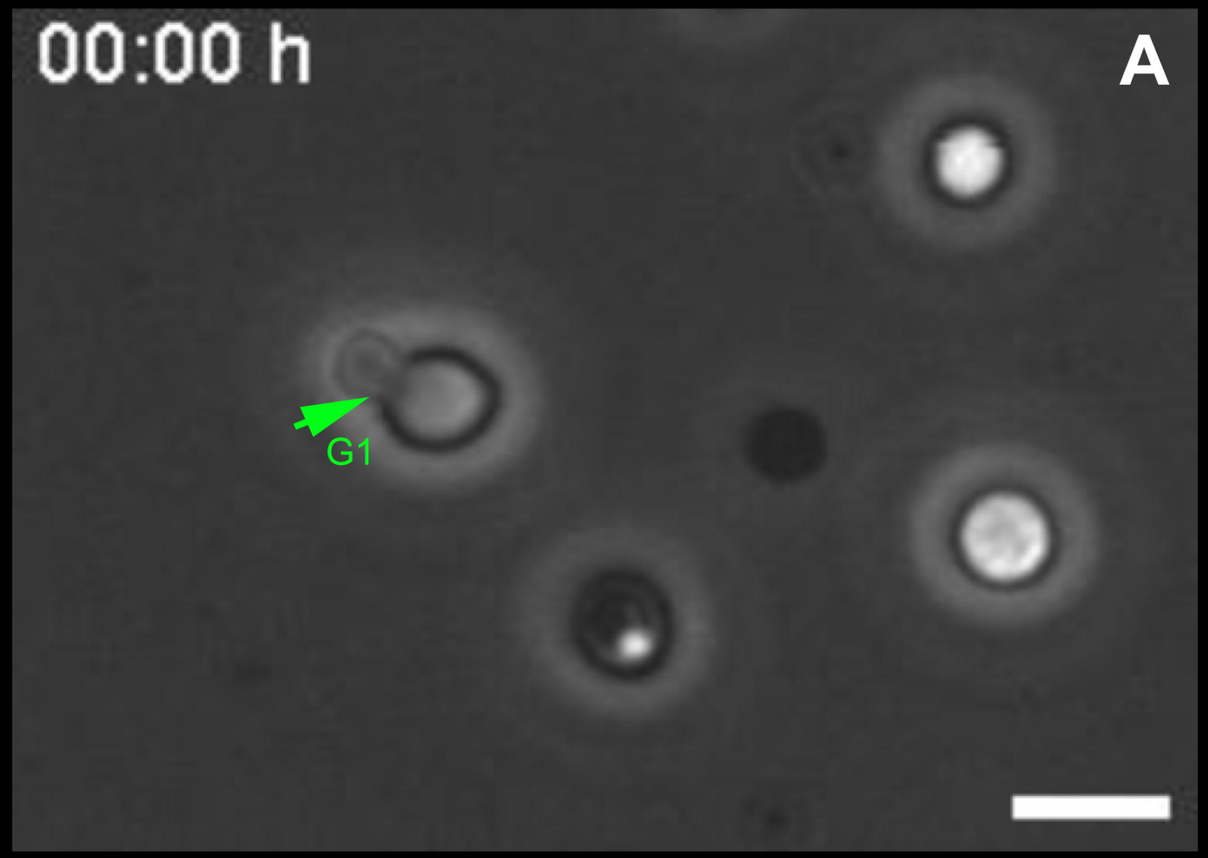
00:00 h
A
G1

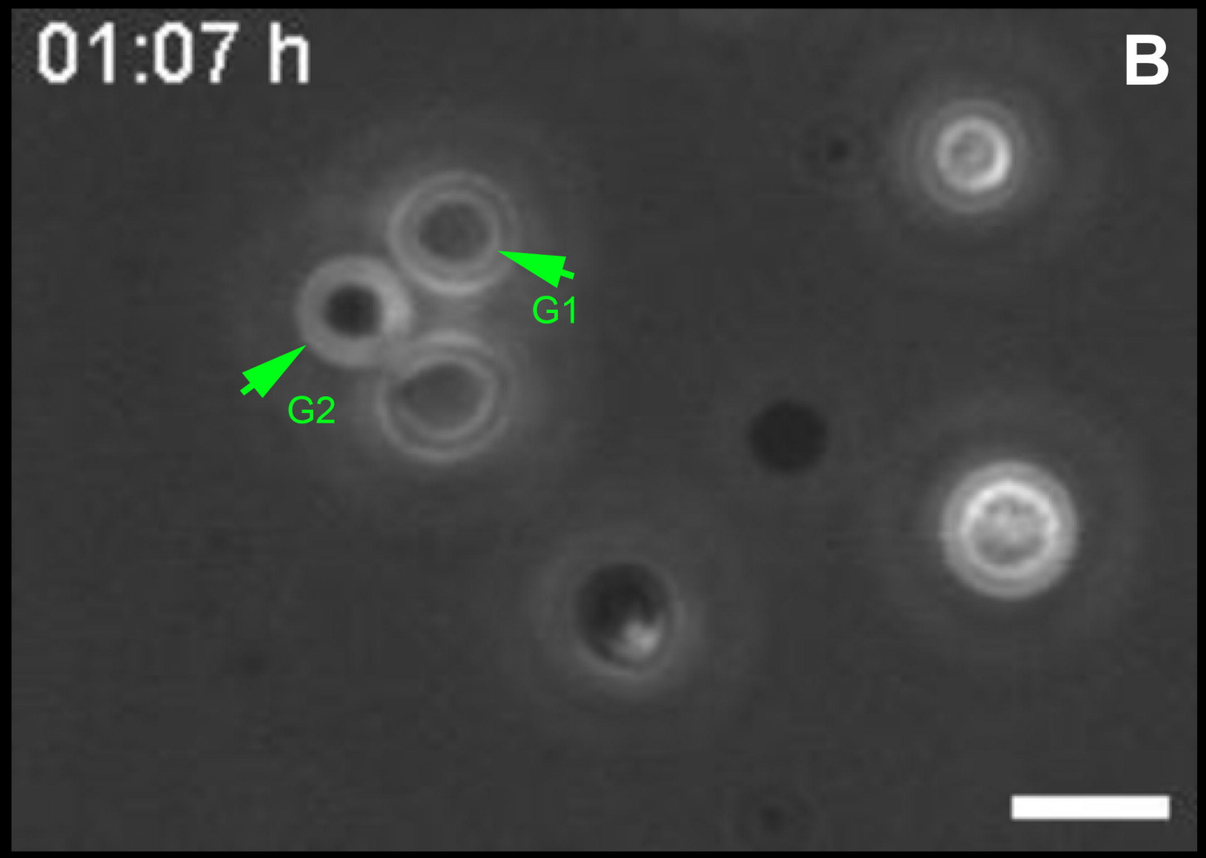
01:07 h
B
G1
G2

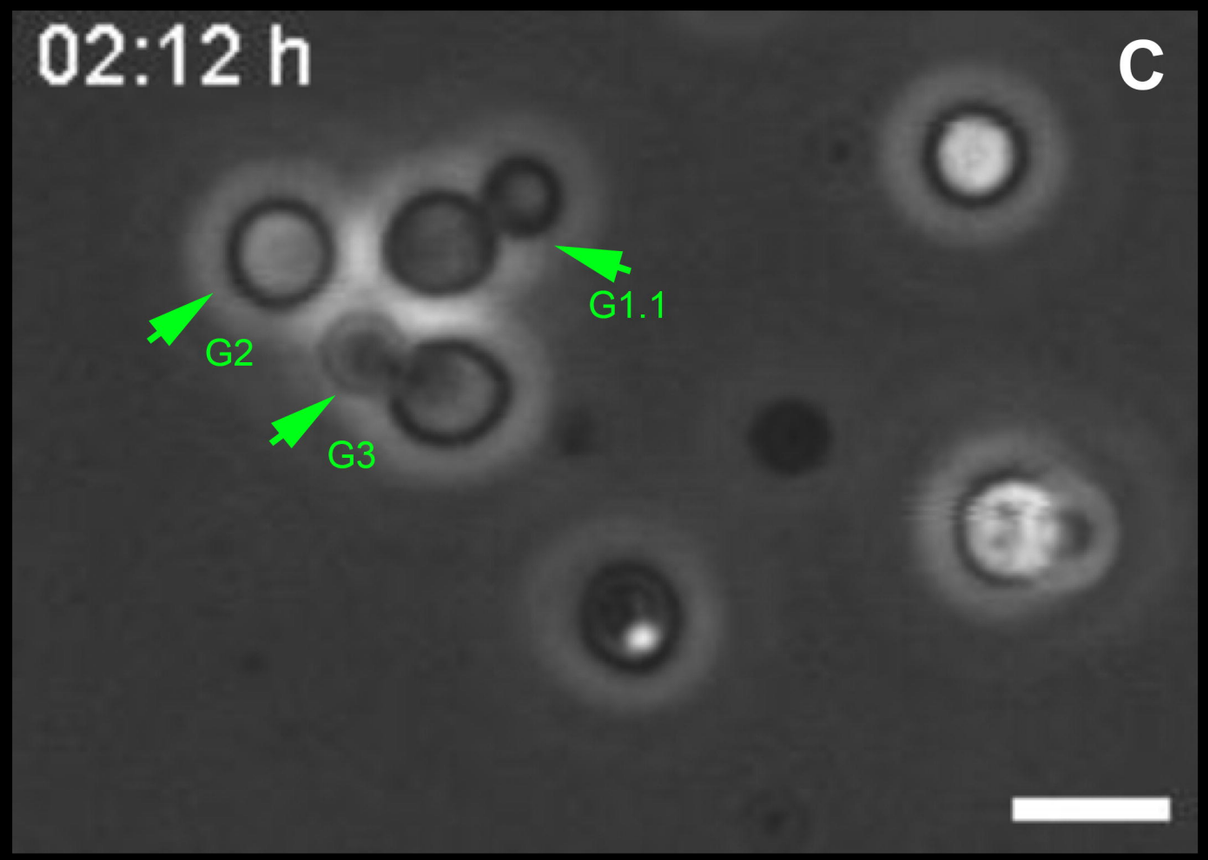
02:12 h
C
G1.1
G2
G3

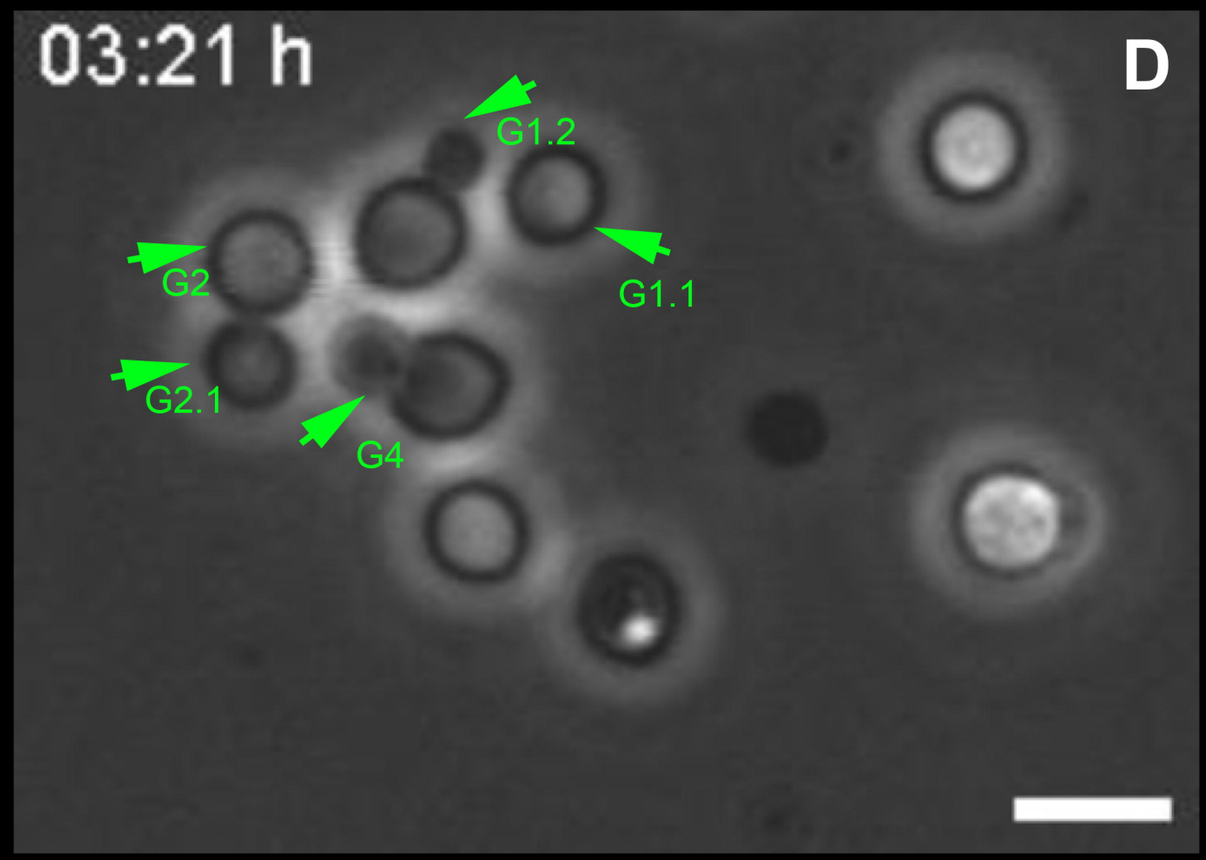
03:21 h
D
G1.2
G2
G1.1
G2.1
G4

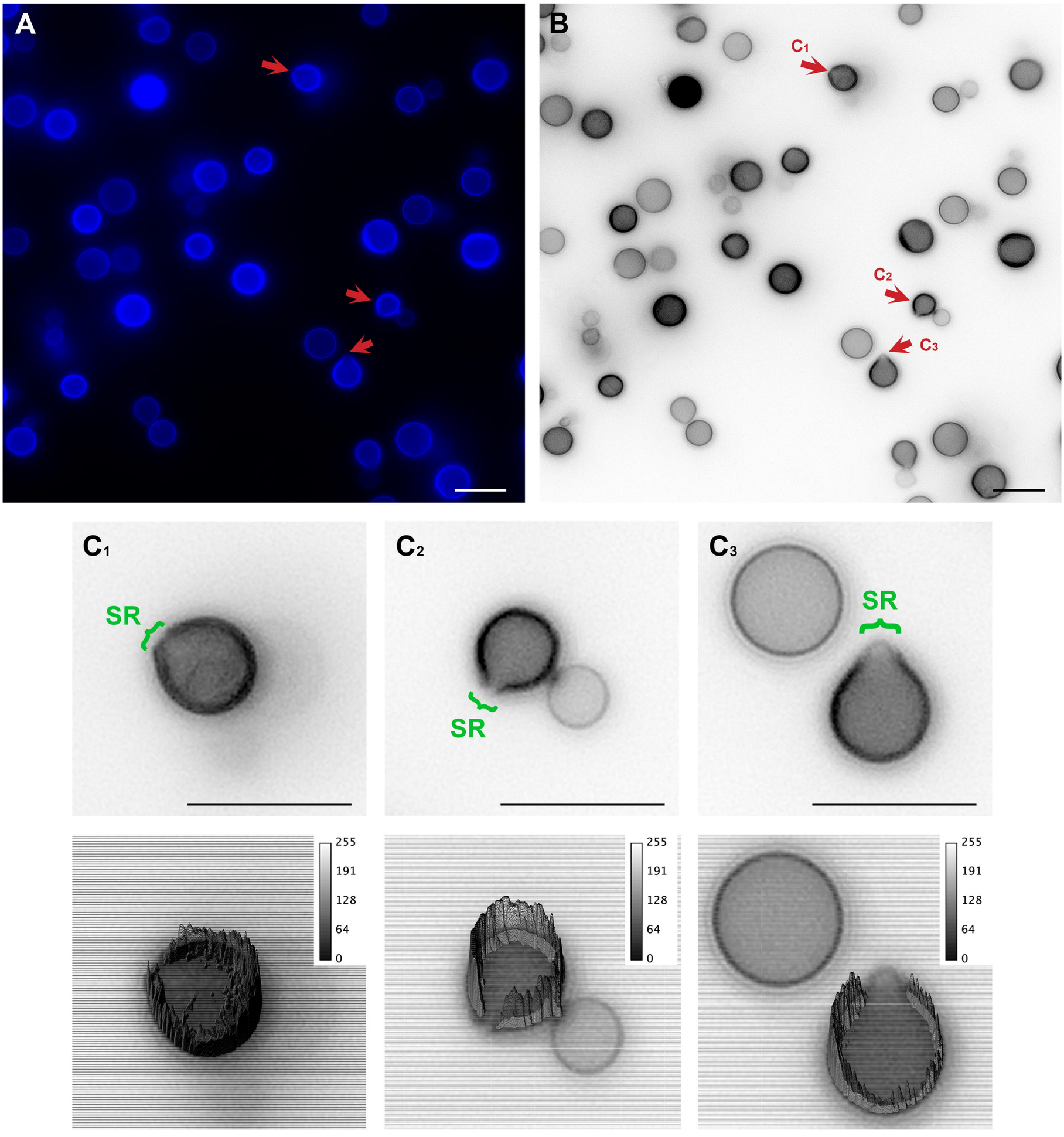
A
B
C1
C2
C3
C1
SR
C2
SR
C3
SR
255
191
128
64
0
255
191
128
64
0
255
191
128
64
0

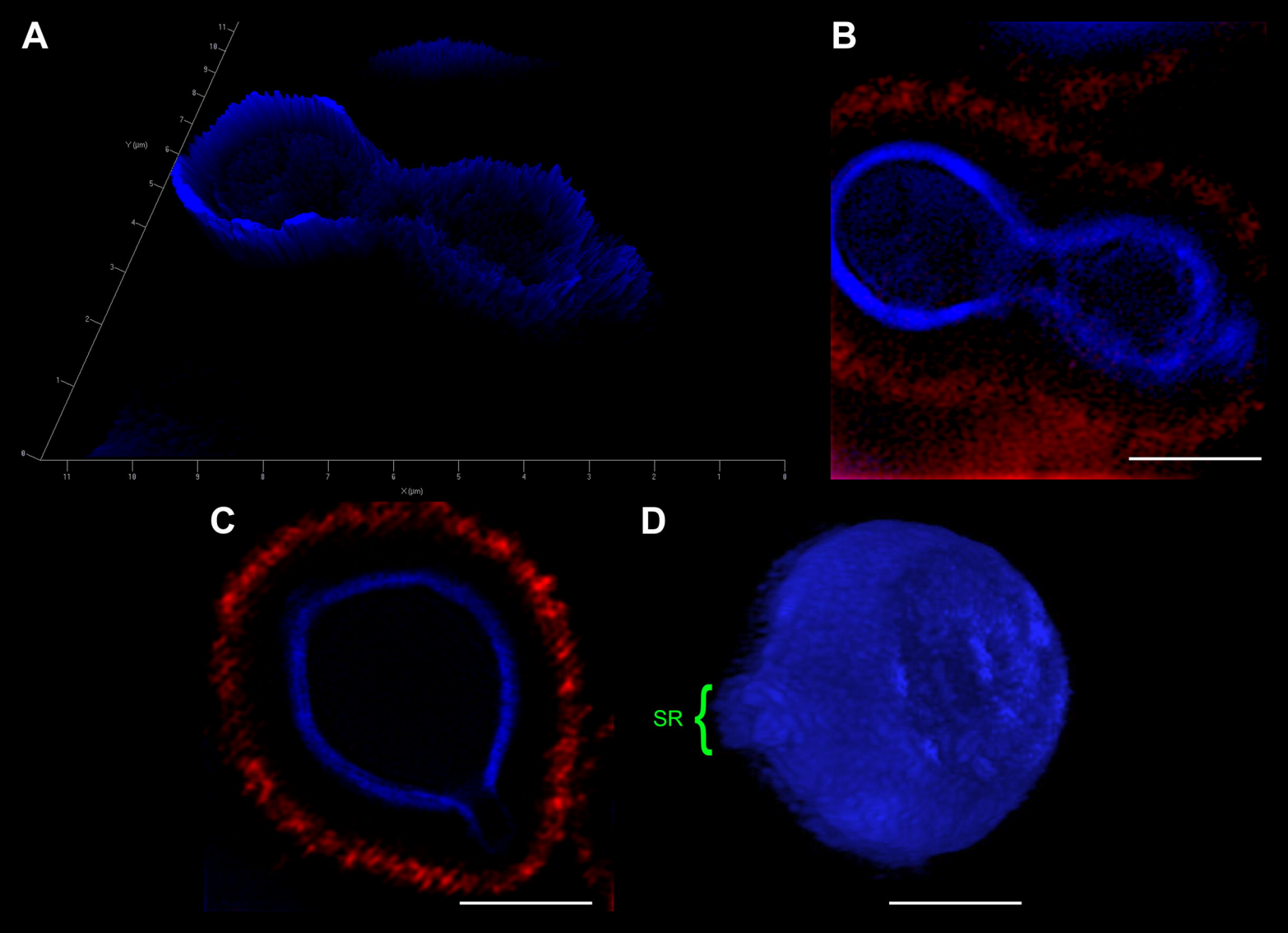
A
B
C
D
SR
Y (µm)
X (µm)

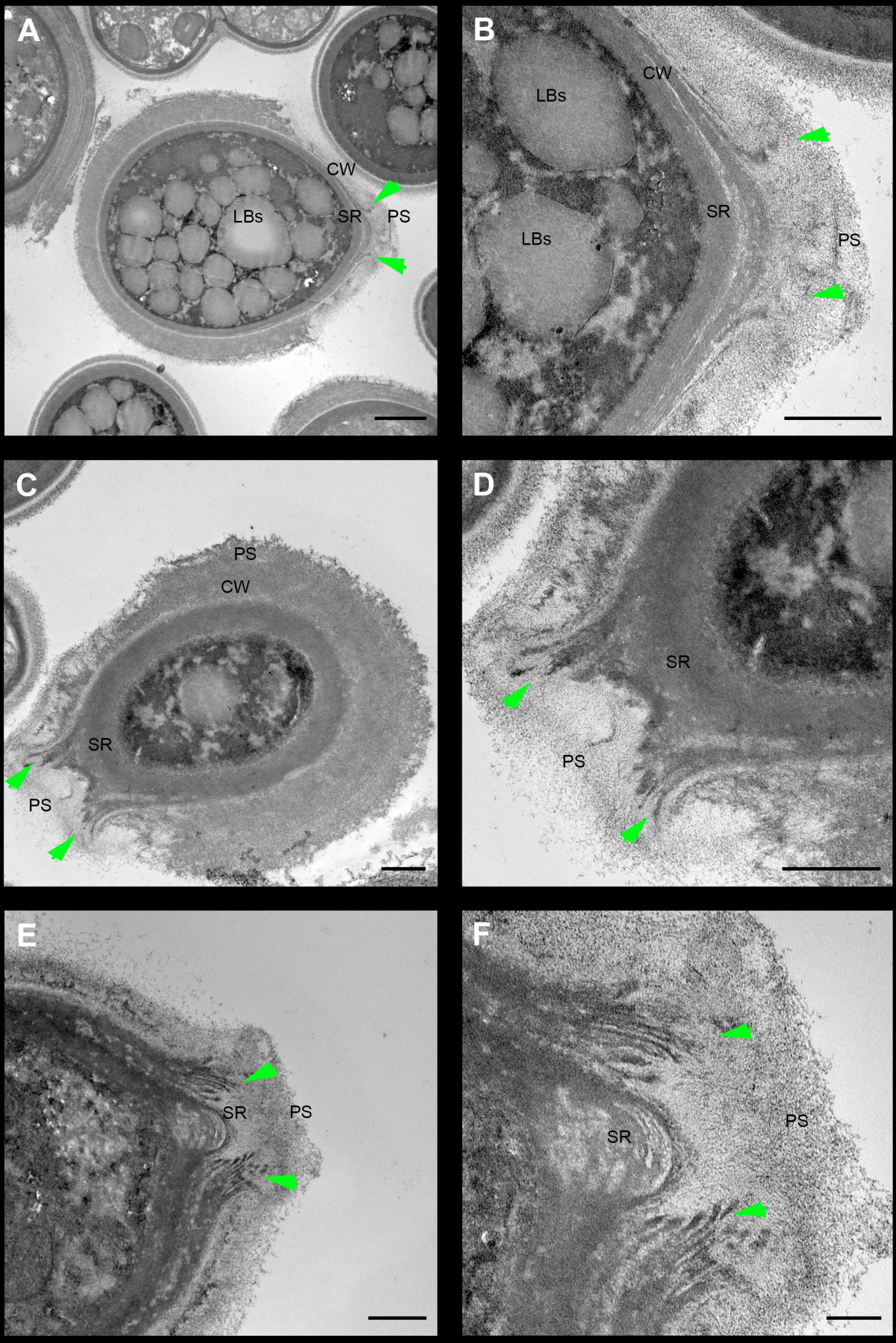
A
CW
LBs
SR
PS
B
CW
LBs
SR
LBs
PS
C
PS
CW
SR
PS
D
SR
PS
E
SR
PS
F
SR
PS